Shear and Extensional Rheology and Flow-Induced Orientation of Carbon Nanofiber/Polystyrene Melt Composites

Koki Miyazono,[1] Christopher D. Kagarise,[1] Kurt W. Koelling,[1] Monon Mahboob,[2] Stephen E. Bechtel[2]

[1]*Department of Chemical and Biomolecular Engineering, The Ohio State University, Columbus, Ohio 43210*
[2]*Department of Mechanical Engineering, The Ohio State University, Columbus, Ohio 43210*

Received 12 February 2010; accepted 6 June 2010
DOI 10.1002/app.32923
Published online 23 August 2010 in Wiley Online Library (wileyonlinelibrary.com).

ABSTRACT: The rheological behavior and morphology of polystyrene/carbon nanofiber (PS/CNF) composites in their melt phase have been characterized through experimental measurements. Viscosity measurements of the PS/CNF composites in the linear viscoelastic regime show the ratio of the transient extensional viscosity to the transient shear viscosity to be greater than three, the Trouton ratio. This behavior is due to differences in the flow-induced orientation of CNFs in shear and extensional flow. The orientation development of the CNFs in shear and extensional flow was analyzed through a method utilizing transmission electron microscopy and was used to explain observed rheological phenomena.
 J Appl Polym Sci 119: 1940–1951, 2011

Key words: nanocomposites; rheology; morphology; orientation; nanofiber

INTRODUCTION

The addition of particles into a polymer matrix is recognized as a simple and effective technique for enhancing the polymer's physical properties while adding new functionality. The ultimate objective for "nanocomposites" (materials that incorporate nanoparticles) is to create high performance materials with lower material costs. Since the discovery of CNFs in 1972[1] and carbon nanotubes (CNTs) in 1991,[2] a tremendous amount of research has been conducted on their use in polymer composites because of the potential to create materials with enhanced mechanical,[3,4] thermal,[5–8] and electrical[9–11] properties, while using much lower particle loadings than traditional microscale fillers such as carbon black, carbon fibers, and glass fibers.[12–16]

In this article, we study the effects of the addition of nanoparticles to a polymer matrix on the transient shear and transient extensional rheology of the composite in the melt phase. The nanoparticles used were carbon nanofibers (CNFs) because they possess many excellent features. Specifically, CNFs are anisotropic, smaller in size and have higher aspect ratios than traditional particles like glass fibers or carbon fibers, they are able to enhance various properties like electrical conductivity and modulus, and have been successfully used in applications such as fuel cells and high performance fibers. Additionally, they cost much less than single-walled-CNTs or multi-walled-CNTs and are considered less of a health hazard than CNTs.[17]

There have been several articles that describe the rheology of polymer/CNF composites using polycarbonate,[18–21] polyethylene,[22] polypropylene,[20,23–30] polyester,[31] polyamide,[23,32] polyimide,[33] poly(methyl methacrylate),[34,35] and polystyrene (PS)[36] as the polymer matrix. Although these articles show the rheological effects of incorporating nanofibers into a polymer matrix, they focus on shear flow and do not investigate the extensional rheology or quantify the effects of fiber orientation.

In previous work, we showed the results of transient and steady-state shear viscosity measurements of PS/CNF composites and validated against the experimental results a constitutive model that predicts the steady-state shear viscosity.[37,38] In this work, we analyze in detail the transient shear and transient extensional rheological responses of the composites and measure the changes in the average nanofiber orientation that occur during flow using a technique developed that makes use of transmission electron microscopy (TEM).

EXPERIMENTAL

Materials

The PS supplied by Chevron Phillips Chemical Company LP (MC3600) was used as received in this study.

Correspondence to: K. W. Koelling (koelling.1@osu.edu).
Contract grant sponsor: National Science Foundation; contract grant number: DMI-0115445.

It has a specific gravity of 1.03, melt flow rate of 13.0 g/10 min (ASTM D 1238 at 200°C, 5 kg polymer). PS was chosen as our thermoplastic polymer matrix because its rheology has been well characterized and any deviation caused by the addition of the CNFs can be readily identified. Furthermore, its molecular structure is simple with no crystalline structure present in the solid phase, thus the structure of the CNFs developed during flow in its molten phase can be preserved when cooled to its solid phase. Also, PS has an aromatic group in its structural unit and can be expected to have high affinity for CNFs. The CNFs are manufactured by Applied Science (Pyrograf III, type PR-24-PS) and were used as-received in this study. The nanofibers obtained were in a powder form consisting largely of fiber agglomerates with most agglomerates less than 1 mm in diameter.

Composite sample preparation

In this study, two methods have been used to prepare CNF/PS composites: melt blending (MB) and solvent casting (SC). This was done to determine whether one method resulted in fibers with larger aspect ratios than the other.

In the MB process, CNF powder and PS pellets were fed into a DACA microcompounder, a small twin-screw extruder with corotating conical screws in which the compounding time, temperature, and screw speed are controlled. It was found that a 5 min compounding time at 200°C and screw rotation rate of 250 rpm achieved good CNF dispersion while minimizing the amount of PS degradation. Polymer degradation was evaluated by measuring the viscosity of the polymer at 200°C for different mixing conditions; higher levels of degradation resulted in polymers with viscosities lower than the virgin material. The composite was extruded from the microcompounder through a 2-mm die and cut into pellets with approximate lengths of 2–3 mm. Composites containing 2, 5, and 10 wt % CNF were prepared by the MB process for this study.

In the SC process, 19.6 g of PS pellets were added to 200 mL of tetrahydrofuran (THF) then stirred for 12 h to create a PS/THF solution. Next, 0.4 g of CNFs were added in the PS/THF solution and sonicated for 15 min by a Sonic Dismembrator (Fisher Scientific, Model: 550; probe: 1″) at 20 kHz and a power level of 550 W L^{-1} while being cooled by ice water. After sonication, the suspensions were cast into films at room temperature to remove most of the solvent. The composite film, still containing some THF solvent, was dried in a vacuum oven at 65°C, broken into small chips having 0.5- to 1-mm diameters by a hand-held Analytical Mill (IKA), and then further dried in a vacuum oven at 65°C for 5 days to remove the remaining THF. Composites containing 2 wt % CNF were prepared using the SC method. In this SC method, no shear deformation in the molten state was applied to the nanocomposite until making molded samples as described later.

Both the MB and SC composite pellets (chips) were compression molded into (1) disks of 25-mm diameter and 0.9- to 1.2-mm thickness for use as shear flow test specimens, and (2) rectangular bars of 52-mm length, 7-mm width, and 1.55-mm thickness for use as elongational flow test specimens. A mold containing the composite pellets or chips was placed in a 200°C press for 15 min to allow the pellets or chips to melt. After the 15 min, pressure was quickly applied and released four times to release air bubbles trapped within the molten composite. The pressure was reapplied and held for 10 min to lock in the shape of the samples, after which the heat supplied to the press was turned off and the pressure was released. The temperature of the sample was allowed to fall below 100°C, the glass transition temperature of the PS. Once the samples cooled, they were removed from the mold. The disks and rectangular bars were stored in a vacuum oven at 65°C for at least 24 h prior to any rheological measurements to prevent the absorption of moisture or air; if stored in open air, bubbles would be generated during melting in the rheometer, which would corrupt the rheological measurements. Two pure PS control samples were prepared: one processed using the MB method and the other using the SC method.

Rheological and morphological characterization

Shear rheology of the melt composites was measured at temperatures of 140°C–200°C in 10°C intervals using a strain-controlled rheometer from TA Instruments (ARES LS2) with both a torque transducer (0.02–2000 g cm) and a normal force transducer (2–2000 g). Parallel plates of 25-mm diameter were used for all measurements. The gap distance was kept in the range 0.9–1.2 mm for all tests. The molded disks were allowed to rest at the measurement temperatures for 15 min so that the polymer could reach thermal equilibrium with the surroundings and to relax the residual stress introduced by the compression molding process. The extensional rheology of the melt composites was measured at 160°C using a RME rheometer from Rheometrics Scientific. The molded rectangular bars, like the disks, were allowed to rest at the measurement temperature for 15 min.

After melting, the samples were stretched to a total strain of 0.1, 0.3, 1, or 3 at a constant extensional rate of 0.01, 0.1, or 1.0 s^{-1}. A FEI Technai G2 Spirit transmission electron microscope (TEM) was used at 100 keV to observe the nanometer-scale CNF dispersion and structure in the composites at 4800× magnification. One sample was left undeformed to

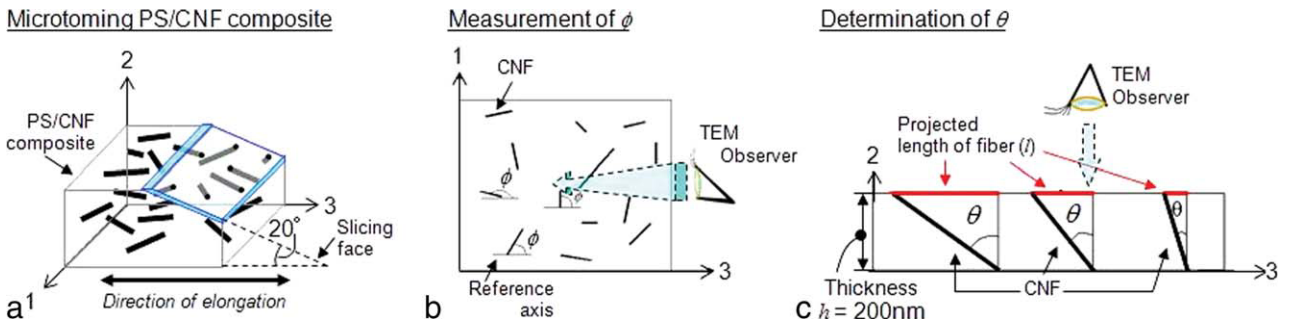

Figure 1 Methods of sample preparation for TEM: (a) microtoming PS/CNF composite; (b) measurement of (ϕ); and (c) determination of (θ). [Color figure can be viewed in the online issue, which is available at wileyonlinelibrary.com.]

determine the initial orientation of the CNFs in the test bars. Each sample was cut with an ultramicrotome at an angle of 20° relative to the stretching direction and to a thickness of 200 nm (Fig. 1) and placed on a copper grid to be viewed with the TEM. The 20° angle of cut used to create microtomed specimens was determined to be the optimum value in our previous work[38] (details of the method used to determine the orientation of CNFs will be described in a later section). An optical microscope (Zeiss Axioskop) was used to observe the state of CNF dispersion at a magnification of 400×.

RESULTS AND DISCUSSION

In this section, we present measurements of CNF morphology and dispersion in the PS matrix and measurements of the bulk rheology of the CNF/PS composites in the melt phase during small-amplitude oscillatory shear, transient shear and transient uniaxial extensional flows.

Morphology and dispersion of CNFs in the polymer matrix

The morphology and dispersion of CNFs in composites prepared by MB and SC methods have been characterized using optical microscopy and TEM. The length of the CNFs after being processed through MB or SC was measured by dissolving the CNF/PS composite in THF with a composite to solvent ratio of about 8 : 100 by weight and viewing a thin film of the resulting THF/CNF/PS suspension with an optical microscope. TEM images were used to measure CNF diameters and their dispersion at micrometer-sized length scales.

Figure 2 shows optical microscopy images of 2 wt % MB and 2 wt % SC composites suspended in THF [Fig. 2(a,b), respectively] and a TEM micrograph of 2 wt % MB composites [Fig. (2c)]. From numerous TEM images of the sections of solidified MB composites, like the one shown in Figure 2(c), at all CNF concentrations, we determined that the CNFs were uniformly dispersed over an area of $2.5 \times 10\ \mu m^2$ in the MB composites. In contrast, over a similar area, we observed regions almost devoid of CNFs in the SC composites, most likely due to CNF settling during the drying process; over an area of $1.0 \times 10^4\ \mu m$ the SC composites exhibit good uniformity.

Figure 3 shows CNF length distributions for 2, 5, and 10 wt % MB and 2 wt % SC composites that were determined from the optical microscopy images. Table I shows the number average CNF length (L_N), weight average CNF length (L_W), the

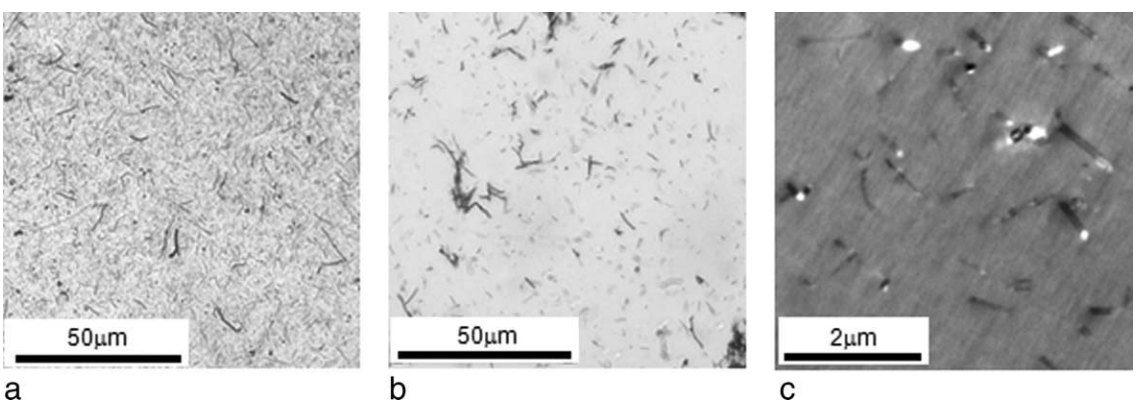

Figure 2 Optical microscopy images (a, b) and TEM micrograph (c) of a 2 wt % composite (a, c: melt blended; b: solvent cast).

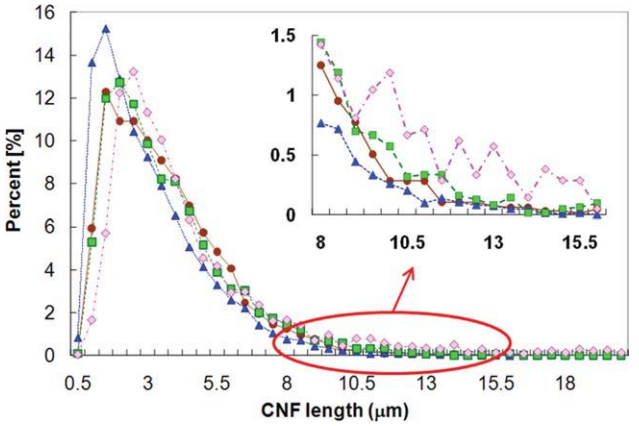

Figure 3 Distribution of CNF length after sample preparation of PS/CNF composites (MB2, solid circle; MB5, solid triangle; MB10, gray square; and SC2, open diamond). [Color figure can be viewed in the online issue, which is available at wileyonlinelibrary.com.]

distribution of CNF lengths for each sample calculated by L_W/L_N and the total percentage of CNFs longer than 10 μm. These results show that there are almost no CNFs longer than 8 μm in the MB composites, an indication that uniform micron scale dispersion is attained at the cost of CNF length. The diameters of the CNFs in both MB and SC composites were measured from TEM images and were found to be in the same 50–150 nm range found for the as-received fibers. Combining the weight average length (L_W) and diameter measurements of 6000 to 12,000 fibers for each composite system, we find that a representative aspect ratio for the MB2 composites is 48 and for the SC2 composites is 80. The distribution of CNF lengths for the MB2 composites is around 1.4 while the distribution for the SC2 composites is 1.8. These results imply that the MB process creates more shear forces than sonication, resulting in longer fibers and a larger distribution of CNF length in the SC samples. The L_W of the CNFs was computed in a similar manner as weight-average molecular weights for polymers.

Linear viscoelasticity

In our linear viscoelastic characterization of the response of the CNF/PS composites to small-amplitude oscillatory shear, we first determined the boundaries of the linear regime over which the storage modulus, G', and loss modulus, G'', are independent of strain amplitude by running strain amplitude sweeps from 0.1% to 10% strain at different frequencies on each sample. The linear viscoelastic region was found to decrease with increasing CNF concentration and/or longer CNF lengths as the boundary of the linear regime was 1% strain for the MB2 and MB5 composites and 0.5% strain for the MB10 and

TABLE I
Analysis of CNF Length after Preparation of PS/CNF Composites

Specimens	L_N (μm)[a]	L_W (μm)[b]	% of long CNFs[c]	Aspect ratio[d]	Distribution[e]
MB, 2 wt %	3.43	4.78	1.56	48	1.39
MB, 5 wt %	2.88	4.38	1.18	44	1.52
MB, 10 wt %	3.49	5.01	2.39	50	1.44
SC, 2 wt %	4.46	8.01	7.86	80	1.80

[a] Number average length of CNFs.
[b] Weight average length of CNFs.
[c] Total percentage of CNFs that are longer than 10 μm.
[d] L_W/diameter of CNF (≈0.1 μm).
[e] Distribution of CNF length for each sample, L_W/L_N.

SC2 composites. This may be evidence that any structure formed by the CNFs is weak; even a small strain may alter the structure causing a nonlinear response.

Figure 4 shows the master curves of storage modulus, G', of the MB and SC composites and samples of pure PS which have undergone the same mixing process as the melt-blended composites (denoted MB0). The G' master curve of the pure polymer that had undergone the SC process (denoted SC0) was found to perfectly corresponded to the MB0 master curve and therefore has been omitted from Figure 4 for simplicity. The small amplitude oscillatory shear experiments were performed over the temperature range of 140°C–200°C. The master curves were generated by shifting the measured data to 160°C following the principles of time–temperature superposition; the shift factors (a_T) of all the MB and SC composites and the pure polymer control samples are plotted in Figure 5. Our measurements show

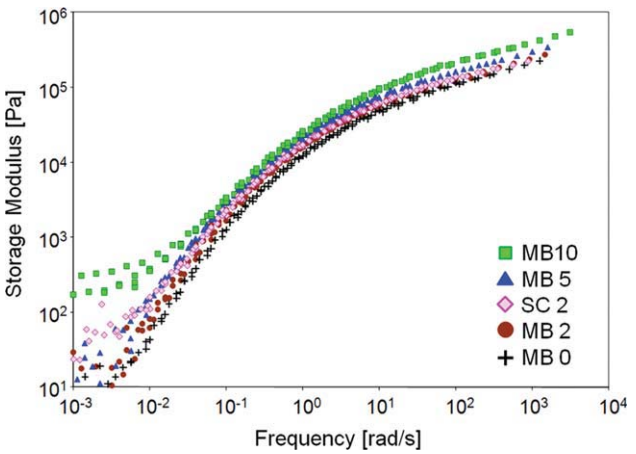

Figure 4 Master curve of elastic modulus (G') for MB and SC composites with CNF concentrations in the MB samples ranging from 0 to 10 wt %, and a CNF concentration of 2 wt % in the SC sample. Data were measured from 140°C to 200°C and shifted to 160°C. [Color figure can be viewed in the online issue, which is available at wileyonlinelibrary.com.]

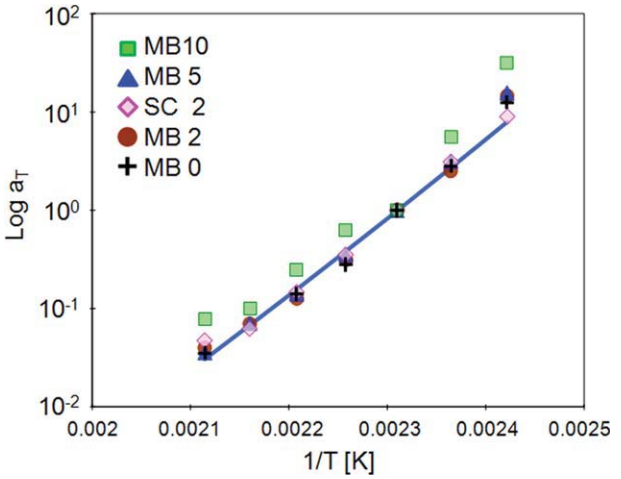

Figure 5 Time-temperature superposition shift factors of MB and SC composites. C1 = 13.7 and C2 = 5055 were used as constants in the Williams-Landel-Ferry (WLF) equation in this study. [Color figure can be viewed in the online issue, which is available at wileyonlinelibrary.com.]

marked effects of the CNFs on the linear viscoelastic moduli, especially at low frequencies (see Figs. 4 and 5). For MB composites, the storage modulus, G', increases monotonically with increasing CNF concentration and a low frequency plateau is especially evident for the MB10 composite. For solvent-cast composites, G' also increases with increasing CNF concentration and in addition a low frequency plateau for SC2 occurs. Moreover, the difference in G' between the SC2 and SC0 (equal to MB0 in Fig. 4) samples is greater than the difference in G' between the MB2 and MB0 samples, which is caused by the greater length of the CNFs in the SC composite samples. At low frequencies, homogeneous polymers typically exhibit the terminal behavior of $G' \propto \omega^2$ and $G'' \propto \omega$, so that the slopes of log G' versus log ω and log G'' versus log ω at low frequencies are equal to 2 and 1, respectively. Table II is a list of the low-frequency slopes of $d(\log G')/d(\log \omega)$ and $d(\log G'')/d(\log \omega)$ deduced from our small-amplitude oscillatory shear measurements on the MB and SC composites and pure PS samples. Both the pure polymer sample that underwent the MB process (MB0) and the pure polymer sample that underwent the SC process (SC0) exhibit the terminal behavior typical of homogeneous polymers, with slopes of G' near 2 and G'' near 1, however the slopes of G' and G'' decrease with increasing CNF concentration. Furthermore, the slopes of G' and G'' for the SC2 composite are smaller than those of the MB5 and MB2 composites, indicating that fiber length can have a greater influence than fiber concentration on the viscoelasticity of the composites. The nonterminal behavior seen in the CNF containing composites is an indication of a solid-like, elastic response with long relaxation times.

Solomon et al.[39] suggested in their research of polypropylene/clay hybrid materials that the low-frequency plateau was the result of non-Brownian network structure formed by individual clay platelets. Pötschke et al.[40] studied multiwalled carbon nanotube (MWNT)/polycarbonate systems and found that a low-frequency plateau in G' occurred when the MWNT loading was 2 wt % or higher. They suggested that the MWNTs form interconnected structures that dominate the rheological behavior at low frequencies. It is likely that during the flow of our CNF/PS melt composites there are interactions between the CNFs. From the data, we collected it appears that the shorter CNFs in the MB composites interact less with each other than the longer CNFs in the SC composites. Continuing this conjecture, the shortness of the CNFs in the MB composites renders them essentially rigid rods that can be confined by their neighboring CNFs such that they limit the rotational degrees of freedom and for which fiber entanglement is almost impossible. In contrast, the longer CNFs in the SC composites can more readily entangle with each other to form a network structure based on physical contact. At higher CNF concentrations and lower frequencies, these structures respond at longer time scales than composites without a CNF structure, producing solid-like behavior. As a result, the decrease in the slope of G' and G'' of the SC composites is more dramatic than that of the MB composites.

The temperature shift factors (shown in Fig. 5) used to create the master curves in Figure 4 following the principle of time-temperature superposition are almost independent of CNF concentration and length and are nearly all equal to those of pure PS[41] except the MB10 composite. (We assume that MB5 is in the semidilute regime and MB10 is in the concentrated regime[37] in this study.) The theoretical foundation of time-temperature superposition is that the relaxation times of the polymer chains have the same temperature dependence.[42] In light of this statement, and noting that the addition of CNFs to the PS does not alter the shift factors, it seems that the mobility of the polymer chains are not constrained by the CNFs. Polymer–nanoclay composites[39] are similar systems in which inorganic

TABLE II
Slopes of $G'(\omega)$ and $G''(\omega)$ at Low Frequencies

	MB composites		SC composites	
Weight percent	$d(\log G')/d(\log \omega)$	$d(\log G'')/d(\log \omega)$	$d(\log G')/d(\log \omega)$	$d(\log G'')/d(\log \omega)$
0	1.92	1.00	1.94	0.97
2	1.73	0.93	1.15	0.84
5	1.26	0.86		
10	1.02	0.77		

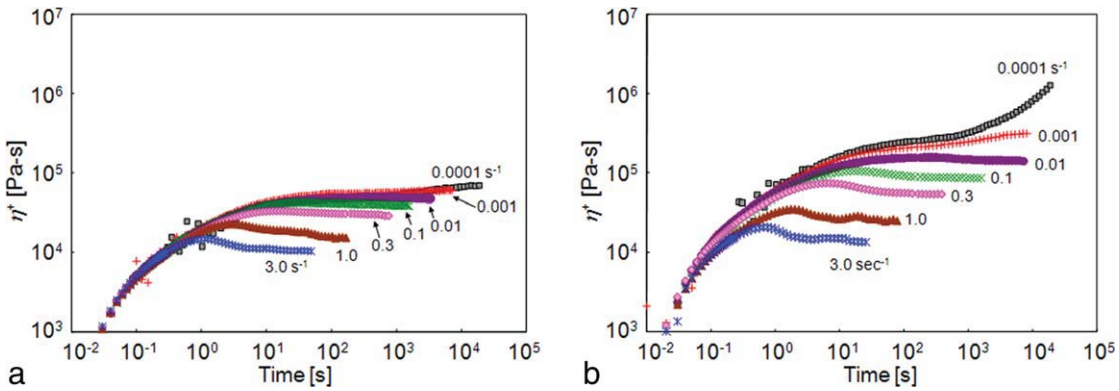

Figure 6 Transient-shear viscosity, η^+, of (a) pure PS and (b) MB10 at shear rates 0.0001–3.0 s^{-1} at $T = 160°C$. [Color figure can be viewed in the online issue, which is available at wileyonlinelibrary.com.]

particles are observed to have marked effects on G' and G'' but not on the shift factors of time-temperature superposition.

Transient shear rheology

Before displaying the transient shear viscosity, η^+, of the PS/CNF melt composites, we show in Figure 6(a) the transient shear viscosity of pure PS (MB0) in the start-up of steady shear over the shear rate range 0.0001–3 s^{-1}. It can be seen that for the pure PS, at small shear rates, the transient viscosity, η^+, gradually increases to steady state and shows a Newtonian plateau at shear rates less than 0.01 s^{-1}. At shear rates greater than 0.01 s^{-1} the polymer is shear thinning, and at shear rates greater than 1.0 s^{-1} the stress values go through a maximum before reaching steady state.

Figure 6(b) shows η^+ for the MB10 composite over the same range of shear rates. Comparing Figures 6(a,b), it is seen that η^+ of MB10 is larger than that of MB0 at the same shear rate, but for shear rates between 0.1 and 10 s^{-1}, the shape of the curves in the two figures is similar. However, instead of displaying the Newtonian plateau in the shear rate range 0.0001–0.01 s^{-1} that was seen in the MB0 sample, the transient viscosity of the MB10 composites increases markedly as strain rate decreases and in some cases steady state was never achieved (shear rates of 0.001 and 0.0001 s^{-1}). For CNF concentrations less than or equal to 2 wt % and at shear rates 0.01 s^{-1} or greater, we observed that the viscosity of the composite reaches a true steady state at an approximate strain of 20. However, for higher concentrations and lower shear rates, the identification of steady-shear viscosity presents some challenges as the viscosity never reaches a steady state in times typical in polymer processing [see Fig. 6(b) in which the viscosity of the MB10 composite at a shear rate of 0.0001 s^{-1} is still evolving after 6 h].

Figure 7 shows the first normal stress coefficient, Ψ_1, as a function of time for the MB0 and MB10 composites over the same range of shear rates. Ψ_1 at shear rates less than 0.01 s^{-1} are not shown because they are too small to be accurately measured. As shown in Figure 7, Ψ_1 decreases monotonically with increasing shear rate and increases with increasing nanofiber concentration. In Figure 7(a), it is seen that the maximum measured value of Ψ_1 for the MB0 composite is $\sim 10^6$ Pa s^2 at a shear rate of 0.1 s^{-1}.

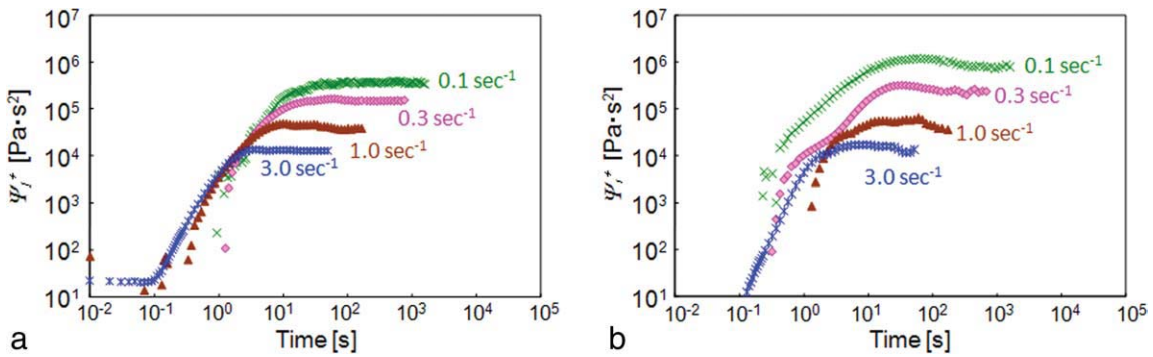

Figure 7 The first normal stress coefficient Ψ_1 of steady shear at shear rates 0.1–3.0 s^{-1} for the (a) MB0 (pure polymer) and (b) MB10 composite, $T = 160°C$. [Color figure can be viewed in the online issue, which is available at wileyonlinelibrary.com.]

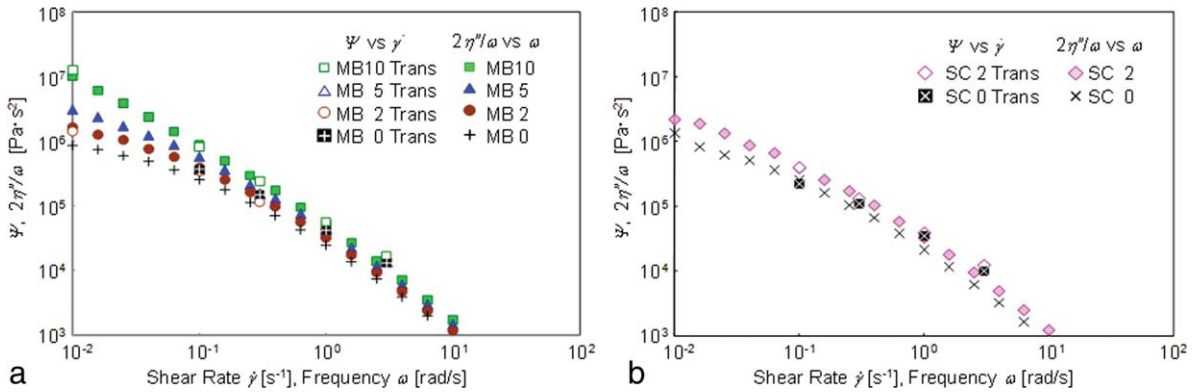

Figure 8 First normal stress coefficient, Ψ_1, vs. shear rate, $\dot{\gamma}$, and $2\eta''/\omega$ vs. ω for (a) MB and (b) SC composites at 160°C. [Color figure can be viewed in the online issue, which is available at wileyonlinelibrary.com.]

The steady-state value of the first normal stress coefficient, Ψ_1, and $2\eta''/\omega$ of the composites as a function of shear rate, $\dot{\gamma}$, and frequency, ω, are displayed in Figure 8(a,b). In the MB and SC composites, Ψ_1 at all CNF concentrations, except MB10, seem to reach a plateau at shear rates or frequencies less than 0.01 s^{-1}. For a given sample, both Ψ_1 and $2\eta''/\omega$ have a similar dependence on shear rate/frequency and are nearly identical at low shear rates.

The characteristic transient shear rheological behavior observed for these composites, decreasing viscosity with increasing shear rate, increasing viscosity with increasing CNF concentration, and a similarity in viscosity of composites of all nanofiber concentrations at high shear rates, can be explained by the same reasoning used to explain the small-amplitude oscillatory shear behavior presented previously. Recall it was suggested that the CNFs create a network structure and as nanofiber concentration increases this network becomes stronger due to the increased contact between fibers. This network structure causes the increase in viscosity with increasing nanofiber concentration. The network structure is affected by shear flow. At low shear rates, the flow of the polymer is slow enough to cause little disruption to the network while at high shear rates the structure is destroyed; hence, at high shear rates the viscosities of all composites are similar.

The transient shear viscosity of the SC2 composites is compared with MB0 and MB2 in Figure 9 over the shear rate range 0.0001–3.0 s^{-1}. At shear rates greater than 0.1 s^{-1} the viscosities of the SC2, MB2, and MB0 are nearly identical. In contrast, at shear rates less than 0.1 s^{-1}, SC2 has a significantly greater viscosity than both MB0 and MB2, and it takes a remarkably long time to reach steady state. These results are, like the response of G' and G'', influenced by the structure formed by CNFs, which appears to be stronger at low shear rates and is due to the greater length of the fibers in the SC2 composite.

Relationship between shear functions

The empirical Cox–Merz rule[43] states that complex viscosity (η^*) versus the dynamic frequency obtained from small-amplitude oscillatory shear is numerically equal to steady-shear viscosity (η) versus the shear rate. Although there is no general explanation for such a relationship, it is widely successful in describing the observed behavior of isotropic polymeric solutions and polymer melts. As η^* is more readily measurable experimentally than η, this rule provides a convenient way to estimate η over a relatively wide range of shear rates. Figure 10 shows that the Cox-Merz rule holds for the MB2 composites, but not for the MB5, MB10, and SC2 composites. Steady-state viscosities of the MB5,

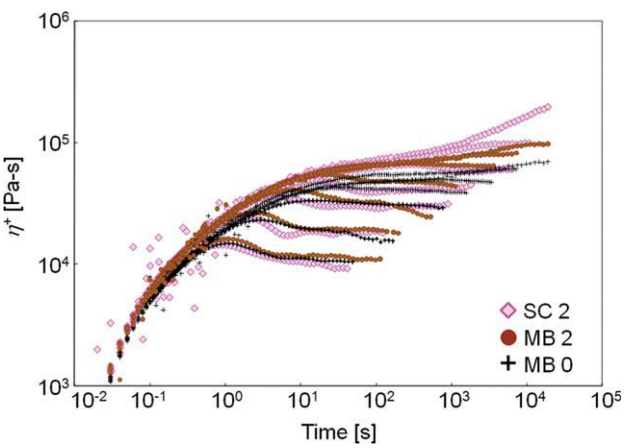

Figure 9 Comparison of transient-shear viscosity, η^+, among MB0, MB2, and SC2 composites at shear rates 0.0001–3.0 s^{-1} and at $T = 160$°C. [Color figure can be viewed in the online issue, which is available at wileyonlinelibrary.com.]

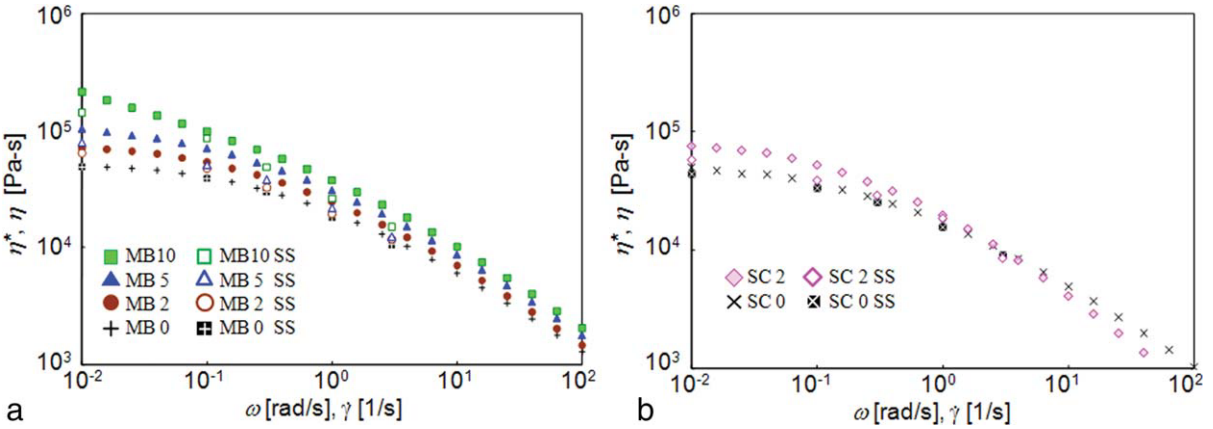

Figure 10 Complex viscosity (η*) vs. frequency (ω) (solid symbols), and steady-shear viscosity (η) vs. shear rate ($\dot{\gamma}$) (open symbols) of (a) MB and (b) SC composites at 160°C. [Color figure can be viewed in the online issue, which is available at wileyonlinelibrary.com.]

MB10, and SC2 composites are significantly less than the corresponding complex viscosity.

Transient extensional viscosity and Trouton's ratio

Figure 11 shows the transient extensional viscosity η_e^+ of pure PS (MB0 and SC0), MB2, MB5, MB10 and SC2 composites over the extension rate range 0.01–1.0 s^{-1}.

A comparison of transient shear viscosity with transient extensional viscosity of the MB2, MB5, and MB10 composites shows the Trouton's ratio (η_e^+/η^+) in the linear viscoelastic regime for each to be greater than three and is calculated in Table III. Pure PS shows the ratio η_e^+/η^+ to be precisely equal to three [solid circle in Fig. 11(a)]. In addition, comparison of the value of η_e^+ for each melt blended sample shows that as CNF concentration increases, η_e^+ and the Trouton's ratio also increase with the exception of the Trouton's ratio for the MB10 composite, which is less than that of MB5 and MB2 (Table III).

Comparing SC2 with SC0, it is seen that the transient extensional viscosity increases with increasing CNF addition as was seen in the MB composites. However, the degree of the increase in extensional viscosity is significantly greater than in MB composites. The transient extensional viscosity of the SC2 sample is almost identical to the extensional viscosity of the MB5 sample; moreover, the Trouton's ratio of SC2 is greater than that of MB5.

The value of steady-state shear viscosity, η, and steady-state extensional viscosity, η_e, in the linear viscoelastic regime and the Trouton's ratio for MB2 and SC2 composites are shown in Table IV. As previously described, the nanofibers in the SC2 composites are distinctly longer than in the MB2 composites, and it is assumed the results shown in Table IV, specifically the ratio of the steady-state extensional viscosities of SC2–MB2 (SS $\eta_e = 1.68$) is significantly greater than the ratio of the steady-state shear viscosities of SC2–MB2 (SS $\eta_s = 1.14$), indicates fiber length has a greater effect on extensional deformation than shear deformation.

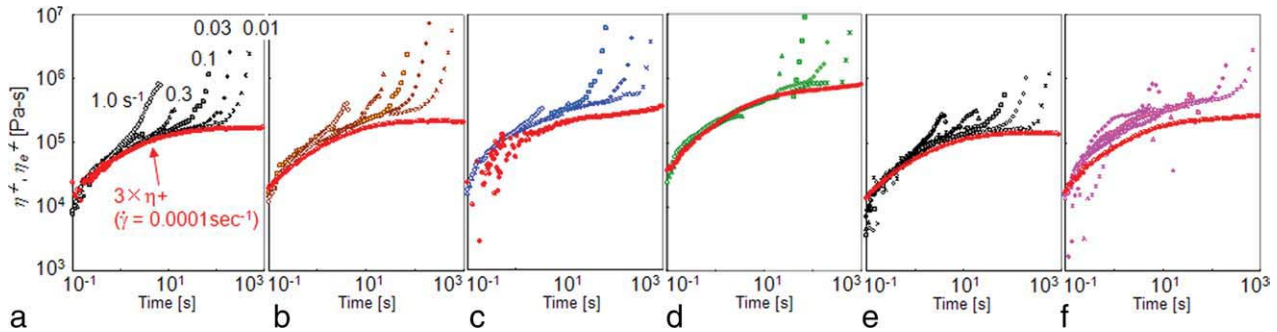

Figure 11 Transient-extensional viscosity, η_e^+, of (a) MB0, (b) MB2, (c) MB5, (d) MB10, (e) SC0, and (f) SC2 at shear rates 0.01 (circle), 0.03 (triangle), 0.1 (square). 0.3 (diamond), and 1.0 s^{-1} (asterisk) at $T = 160$°C. The solid circle is three-times the transient shear viscosity of the same polymer or PS/CNF composite measured at a shear rate of 0.0001 s^{-1}. Data for MB10 are reported for shorter times due to heterogeneous deformation. [Color figure can be viewed in the online issue, which is available at wileyonlinelibrary.com.]

TABLE III
Trouton's Ratio of MB and SC Composites

	MB composites				SC composites	
Weight percent	0	2	5	10	0	2
Trouton's ratio	3.0	3.9	4.6	3.8	3.1	5.8

Batchelor's theory

As previously described, Trouton's ratio (hereinafter "TR") is one of the most important and indicative parameters which imply the effects of the CNFs for both shear and elongational deformation and the resulting viscosities. The TR can be estimated by means of a well-known formula developed by Batchelor (Batchelor's theory).[44–46] The Batchelor's theory model has been extended from the original equation used to describe the TR ratio in polymer suspensions to produce an equation that calculates the TR for polymer mixtures containing anisotropic particles. This equation is given as:

$$\mathrm{TR} = \frac{4}{3}\frac{\phi(l/d)^2}{\ln(\pi/\phi)} \tag{1}$$

where ϕ is the volume fraction of the particles, l is the length of the particle, and d is the diameter of the particle. Volume fraction is calculated by $\phi = n\pi d^2\, l/4$, where n is the number of particles in a unit volume. In eq. (1), there are two assumptions: the length, l, of the rod-like particles is much greater than the distance, h, between parallel particles, and h is much greater than the diameter, d, of the particles, that is to say, $d \ll h \ll l$.

The TR was calculated using eq. (1) using either the number average (L_N) or weight average lengths (L_W) of the CNFs and compared with the experimentally measured TR. These results are given in Table V. It was found that the experimentally measured values of TR were more accurately predicted when using L_N compared with L_W. One exception to this is that there is a remarkably large deviation in the predicted and experimentally measured values for MB10, which could be caused by the invalidity of the assumption $d \ll h$, which is to say the CNFs are too close together. Therefore, from these results, we can say that the Batchelor's theory equation can be applied to molten polymer nanocomposites CNF concentrations of 5 wt % or less.

TABLE IV
Comparison of Steady-State Shear Viscosity η and Steady-State Extensional Viscosity η_e for MB2 and SC2 Composites in the Linear Viscoelastic Regime

	MB 2	SC 2	Ratio
SS η	67,200	76,400	1.14
SS η_e	264,000	444,000	1.68
Trouton's ratio	3.9	5.8	

TABLE V
Experimental and Batchelor's Theory Calculated Values of Trouton's Ratios for MB2, MB5, MB10, and SC2 Composites Using the Weight Average Length (L_W) and Number Average Length (L_N) of the CNFs

Composites	Calculated from L_W	Calculated from L_N	Experimental from η_e^+/η^+
MB 2	5.5	2.8	3.9
MB 5	14.1	6.1	4.6
MB 10	44.4	21.5	3.8
SC 2	15.5	4.8	5.8

Morphology and analysis of CNFs in shear and extensional flow

In this section, we will present a brief description of a method developed to measure the nanoscale structure of the polymer/CNF composites used in this study along with experimental measurement of nanostructure and its evolution during shear and extensional flow to increase the understanding of its influences on rheological properties. Recently, we have found that conventional models that have been applied to predict the orientation evolution of macroscale particles[47,48] in melt composites during flow can be applied to microscale and nanoscale particle suspensions and composites and have suggested[37,49] models to predict rheological properties of nanocomposites using the orientation tensor a_{ij}.

The orientation tensor a_{ij} indicates the orientation of anisotropic particles in three dimensions as shown in Figure 12 and is defined by eq. (2)[48]:

$$a_{ij} = \int_{\phi=0}^{2\pi}\int_{\theta=0}^{\pi} p_i p_j \psi(\phi,\theta)\sin\theta d\theta d\phi \tag{2}$$

where p is a unit vector and ψ is the probability distribution function. As seen in Figure 12, if the particles in a composite are randomly oriented, the values of the diagonal components of the orientation

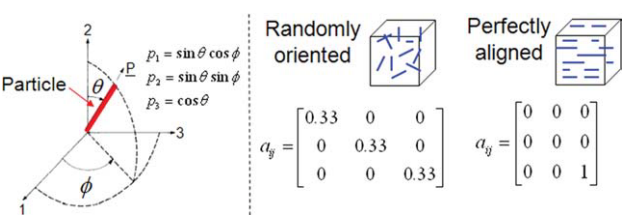

Figure 12 Coordinate diagram of an anisotropic particle (CNF) and the description of the vector p and examples of the orientation tensor a_{ij}. [Color figure can be viewed in the online issue, which is available at wileyonlinelibrary.com.]

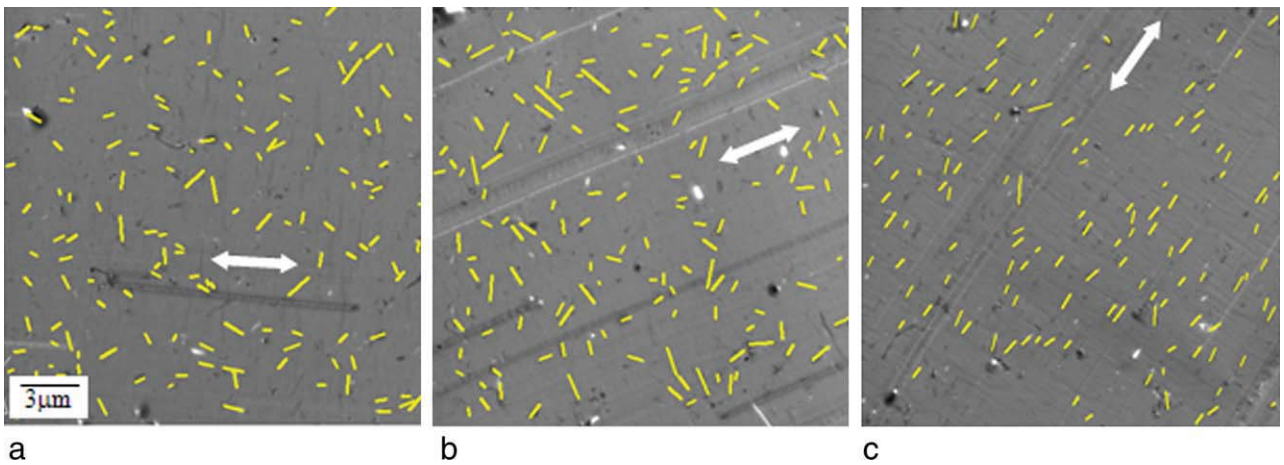

Figure 13 TEM micrographs of MB2 composites (a) before undergoing any deformation (b) under shear flow at a shear rate of 10 s^{-1} and total strain of 70 and (c) under extensional flow at an extension rate of 0.01 s^{-1} and total strain of 3.0. The white arrows indicate the direction of flow and the yellow lines are digitized CNFs. [Color figure can be viewed in the online issue, which is available at wileyonlinelibrary.com.]

tensor are equal to 0.33, and if the particles are perfectly aligned in one direction the value of the a_{ij} component for that direction, in this case a_{33}, is equal to one while all other components are equal to zero. To experimentally measure orientation tensors, the value of two angles, θ and ϕ, need to be determined.

A procedure to determine the value of angles θ and ϕ was developed using a single 2D TEM image as shown in Figure 1. This method relies on two assumptions: the angle ϕ for each fiber can be directly measured from the TEM image by measuring the angle the fiber makes with a reference axis [Fig. 1(b)], and the angle θ can be determined by measuring the projected length of each fiber in the TEM image [Fig. 1(c)] then calculating θ from eq. (3)

$$\theta = \tan^{-1}\left(\frac{l}{h}\right) \tag{3}$$

where l is the projected length of a fiber seen in the TEM picture and h is the thickness of the TEM section. Additional details of the experimental method are available in a previous article.[38]

This method was used to measure the orientation tensor for MB2 composites undergoing shear and extensional flow and SC2 composites undergoing extensional flow. Samples were subjected to shear rates of 0.01, 0.3, and 10 s^{-1} for total strains of 0, 3, and 70 and extension rates of 0.01, 0.1, and 1 s^{-1} for total strains of 0, 0.1, 1, 2, and 3.

Figure 13 shows TEM micrographs of a 2 wt % MB composite (a) before being subjected to flow, (b) after shearing at a shear rate of 10 s^{-1} to a total strain of 70, and (c) after extensional flow at an extension rate of 0.01 s^{-1} to a total strain of 3. The CNFs in the images were overlaid with straight lines using AutoCAD and the lengths and angles of the lines with respect to a baseline were calculated using functions provided by the AutoCAD software. An Auto-LISP code was used to automate the collection of the data and the orientation tensors were calculated.

The experimentally measured values of the orientation tensor component a_{33} (the component

TABLE VI
Experimentally Measured Values of the Orientation Tensor Component a_{33} for MB2 and SC2 Composites at Each Strain, Shear Rate, and Extensional Rate

	MB2 Composites						SC2 composites		
	Shear rate (s^{-1})			Extension rate (s^{-1})			Extension rate (s^{-1})		
Strain	0.01	0.3	10	0.01	0.10	1.0	0.01	0.10	1.0
0	0.443 (common)			0.586 (common)			0.528 (common)		
0.1	–	–	–	0.527	0.580	–	–	–	–
0.3	–	–	–	–	–	–	–	0.773	–
1.0	–	–	–	0.840	0.929	0.881	0.872	0.720	0.873
2.0	–	–	–	0.899	–	0.831	–	–	–
3.0	0.662	–	0.628	0.928	0.940	0.940	0.909	0.890	–
70	0.623	0.428	0.503	–	–	–	–	–	–

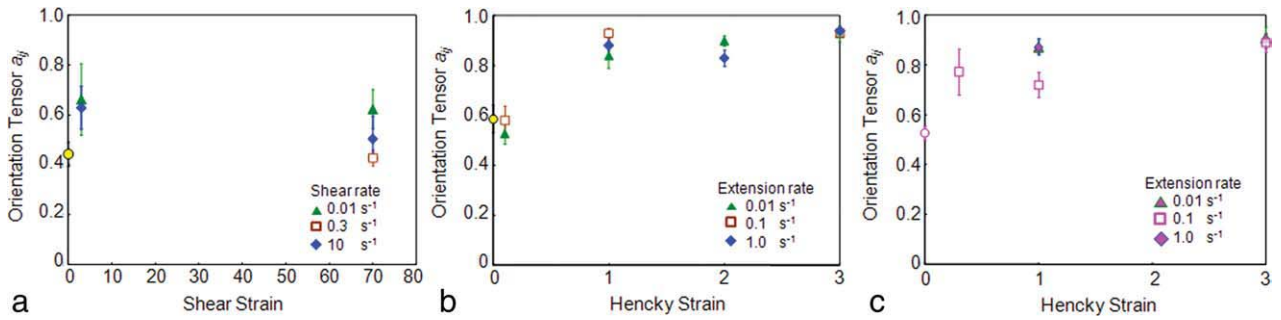

Figure 14 Experimentally measured values of the orientation tensor component a_{33} for (a) MB2 under shear flow, (b) SC2 under extensional flow, and (c) MB2 under extensional flow. Error bars show the standard deviation for each plotted value. [Color figure can be viewed in the online issue, which is available at wileyonlinelibrary.com.]

corresponding to the direction of flow) calculated from the TEM images for both shear and extensional flow are given in Table VI and graphed in Figure 14. The values reported in this table are averages from two TEM images taken at different locations within the sample. From the table and figure, several points can be made. The initial CNF orientation was not completely random as expected which would have been indicated by diagonal components of the orientation tensor being equal to 1/3. There could be several possibilities to explain this. Because the test samples were created from pellets made in a microcompounder, the process of creating the pellets most likely induced some alignment of the nanofibers within the pellets. Because of the size of the pellets relative to the size of the molds it was difficult to totally randomize the orientation of the pellets in three dimensions therefore the test samples did not contain completely randomized nanofibers. It is also possible that the fibers within the sample were totally random however only a small area of the total sample was viewed with the TEM micrograph and the orientation of the nanofibers within that small area were not totally random.

It is also apparent from Table VI and Figure 14 that as strain increases the orientation of the fibers in the direction of the applied strain also increases. Interestingly, there seems to be little relationship between strain rate and the amount of orientation achieved during flow for both shear and extensional flow; however, total strain appears to be important. The strain dependence and strain rate independence of particle orientation has also been observed by those studying glass fiber/polymer composites.[50,51] The orientation evolution of glass fibers in uniaxial extensional flow observed by Wagner et al. further corresponds with our results in that fiber orientation seems to reach a steady state around a total strain of 251. It should also be noted that type of flow is important in that there is a significant difference in the degree of orientation achieved during shear and extensional flows. During shear flow, the average value of the orientation tensor component a_{33} at steady state is $\sim$ 0.5 while for extensional flow that value is $\sim$ 0.9. In the case of extensional deformation, CNFs in the nanocomposites are readily oriented toward the direction applied strain, however, in the case of the shear deformation, the shearing forces cause the CNFs to rotate and/or tumble (Fig. 15) which prevents the formation of a highly oriented structure. These differences in orientation for shear and extensional flow could also help explain the deviation of Trouton's ratio from a value of three that was described in the section "Transient extensional viscosity and Trouton's ratio."

CONCLUSIONS

The rheological behavior and morphology of PS/CNF composites in their melt phase have been studied through experimental measurements. The results show that both shear and extensional viscosities increase with increasing nanofiber concentration. Viscosity measurements of the PS/CNF composites in the linear regime show the ratio of the transient extensional viscosity to the transient shear viscosity to be 3.8 $\sim$ 4.6 (MB composites) and 5.8 (SC composites), which is greater than Trouton's ratio of three. This behavior is due to differences in the flow-induced orientation of the CNFs in shear and extensional flow.

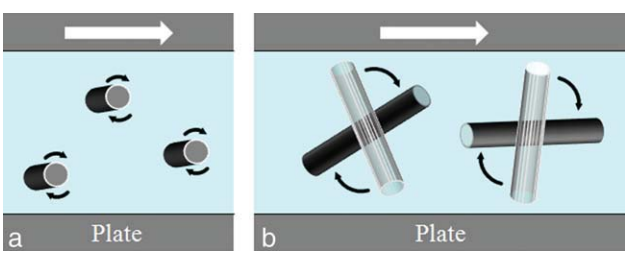

Figure 15 Motion of CNFs in polymer matrices in shear deformation: (a) rotation and (b) tumbling. [Color figure can be viewed in the online issue, which is available at wileyonlinelibrary.com.]

The three-dimensional changes in CNF orientation that occur during flow were measured and quantified using TEM micrographs for both shear and extensional flows at a variety of strain rates and strain. From these measurements, it was observed that CNFs were more aligned in the direction of flow during extensional flow compared with shear flow as a result of shear induced rotation and/or tumbling of CNFs.

The authors thank Dr. Richard Montione, Senior Electron Microscopist of Campus Microscopy and Imaging Facility (CMIF) in the Ohio State University for assistance in acquiring TEM images.

References

1. Koyama, T. Carbon 1972, 10, 757.
2. Iijima, S. Nature (London) 1991, 354, 56.
3. Dyke, C. A.; Tour, J. M. J Phys Chem A 2004, 108, 11151.
4. Geng, H.; Rosen, R.; Zheng, B.; Shimoda, H.; Fleming, L.; Liu, J.; Zhou, O. Adv Mater 2002, 14, 1387.
5. Biercuk, M. J.; Llaguno, M. C.; Radosavljevic, M.; Hyun, J. K.; Johnson, A. T.; Fischer, J. E. Appl Phys Lett 2002, 80, 2767.
6. Choi, E. S.; Brooks, J. S.; Eaton, D. L.; Al-Haik, M. S.; Hussaini, M. Y.; Garmestani, H.; Li, D.; Dahmen, K. J Appl Phys 2003, 94, 6034.
7. Du, F.; Guthy, C.; Kashiwagi, T.; Fischer, J. E.; Winey, K. I. J Polym Sci Part B: Polym Phys 2006, 44, 1513.
8. Yang, S.; Lozano, K.; Lomeli, A.; Foltz, H. D.; Jones, R. Composites Part A 2005, 36, 691.
9. Ramasubramaniam, R.; Chen, J.; Liu, H. Appl Phys Lett 2003, 83, 2928.
10. Meincke, O.; Kaempfer, D.; Weickmann, H.; Friedrich, C.; Vathauer, M.; Warth, H. Polymer 2004, 45, 739.
11. Jiang, X.; Bin, Y.; Matsuo, M. Polymer 2005, 46, 7418.
12. Chan, Y.; White, J. L.; Oyanagi, Y. J Rheol 1978, 22, 507.
13. Lobe, W. M.; White, J. L. Polym Eng Sci 1979, 19, 617.
14. Tanaka, H.; White, J. L. Polym Eng Sci 1980, 20, 949.
15. Lin, G.; Hu, M. Adv Polym Tech 1997, 16, 199.
16. Mobuchon, C.; Carreau, P. J.; Heuzey, M.-C.; Sepehr, M. Polym Compos 2005, 26, 247.
17. Shvedova, A. A.; Kisin, E. R.; Mercer, R.; Murray, A. R.; Johnson, V. J.; Potapovich, A. I.; Tyurina, Y. Y.; Gorelik, O.; Arepalli, S.; Schwegler-Berry, D.; Hubbs, A. F.; Antonini, J.; Evans, D. E.; Ku, B.-K.; Ramsey, D.; Maynard, A.; Kagan, V. E.; Castranova, V.; Baron, P. Am J Physiol Lung Cell Mol Physiol 2005, 289, L698.
18. Caldeira, G.; Maia, J. M.; Carneiro, O. S.; Covas, J. A.; Bernardo, C. A. Polym Compos 1998, 19, 147.
19. Carneiro, O. S.; Covas, J. A.; Bernardo, C. A.; Caldeira, G.; Van Hattum, F. W. J.; Ting, J.-M.; Alig, R. L.; Lake, M. L. Compos Sci Technol 1998, 58, 401.
20. Hammel, E.; Tang, X.; Trampert, M.; Schmitt, T.; Mauthner, K.; Eder, A.; Pötschke, P. Carbon 2004, 42, 1153.
21. Higgins, B. A.; Brittain, W. J. Eur Polym J. 2005, 41, 889.
22. Lozano, K.; Yang, S.; Zeng, Q. J Appl Polym Sci 2004, 93, 155.
23. Tibbetts, G. G.; McHugh, J. J. J Mater Res 1999, 14, 2871.
24. Van Hattum, F. W. J.; Bernardo, C. A.; Finegan, J. C.; Tibbetts, G. G.; Alig, R. L.; Lake, M. L. Polym Compos 1999, 20, 683.
25. Carneiro, O. S.; Maia, J. M. Polym Compos 2000, 21, 960.
26. Lozano, K.; Barrera, E. V. J Appl Polym Sci 2001, 79, 125.
27. Lozano, K.; Bonilla-Rios, J.; Barrera, E. V. J Appl Polym Sci 2001, 80, 1162.
28. Ceccia, S.; Ferri, D.; Tabuani, D.; Maffettone, P. L. Rheol Acta 2008, 47, 425.
29. Kumar, S.; Doshi, H.; Srinivasarao, M.; Park, J. O.; Schiraldi, D. A. Polymer 2002, 43, 1701.
30. Carneiro, O. S.; Maia, J. M. Polym Compos 2000, 21, 970.
31. Ma, H.; Zeng, J.; Realff, M. L.; Kumar, S.; Schiraldi, D. A. Compos Sci Technol 2003, 63, 1617.
32. Lake, M. L.; Glasgow, D. G.; Kwag, C.; Burton, D. J. In Proceedings of 47th International SAMPE Symposium and Exhibition; Society for the Advancement of Material and Process Engineering, Covina, California, 2002; p 1794.
33. Glasgow, D. G.; Tibbetts, G. G.; Matuszewski, M. J.; Walters, K. R.; Lake, M. L. In Proceedings of 49th International SAMPE Symposium and Exhibition; Society for the Advancement of Material and Process Engineering, Covina, California, 2004; p 2355.
34. Cooper, C. A.; Ravich, D.; Lips, D.; Mayer, J.; Wagner, H. D. Compos Sci Technol 2002, 62, 1105.
35. Zeng, J.; Saltysiak, B.; Johnson, W. S.; Schiraldi, D. A.; Kumar, S. Composites Part B 2004, 35, 173.
36. Cipriano, B. H.; Kota, A. K.; Gershon, A. L.; Laskowski, C. J.; Kashiwagi, T.; Bruck, H. A.; Raghavan, S. R. Polymer 2008, 49, 4846.
37. Wang, Y.; Xu, J.; Bechtel, S. E.; Koelling, K. W. Rheol Acta 2006, 45, 919.
38. Mahboob, M.; Kagarise, C.; Koelling, K. W.; Bechtel, S. E. Polym Compos, to appear.
39. Solomon, M. J.; Almusallam, A. S.; Seefeldt, K. F.; Somwangthanaroj, A.; Varadan, P. Macromolecules 2001, 34, 1864.
40. Pötschke, P.; Fornes, T. D.; Paul, D. R. Polymer 2002, 43, 3247.
41. Macosko, C. W. Rheology; Principles, Measurements and Applications; Wiley-VCH: New York, 1994.
42. Ferry, J. D. Viscoelastic Properties of Polymers; Wiley: New York, 1980.
43. Cox, W. P.; Merz, E. H. J Polym Sci 1958, 28, 619.
44. Batchelor, G. K. J Fluid Mech 1971, 46, 813.
45. James, D. F.; Sridhar, T. J Rheol 1995, 39, 713.
46. Lubansky, A. S.; Boger, D. V.; Cooper-White, J. J. J Non-Newt Fluid Mech 2005, 130, 57.
47. Tucker, C. L. J Non-Newton Fluid Mech 1991, 39, 239.
48. Advani, S. G.; Tucker, C. L. J Rheol 1987, 31, 751.
49. Kagarise, C.; Koelling, K. W.; Wang, Y.; Bechtel, S. E. Rheol Acta 2008, 47, 1061.
50. Kobayashi, M.; Takahashi, T.; Takimoto, J.; Koyama, K. Polymer 1995, 36, 3927.
51. Wagner, A. H.; Kalyon, D. M.; Yazici, R.; Fiske, T. J. J Reinf Plast Compos 2003, 22, 327.